Efficient Reduction of Powerline Signals in Magnetic Data Acquired From a Moving Platform

M. Andy Kass, Anders Vest Christiansen, Esben Auken, and Jakob Juul Larsen, *Senior Member, IEEE*

***Abstract*— High-bandwidth magnetic data are normally distorted by ubiquitous 50- or 60-Hz noise from powerlines and similar sources. The powerline noise can be orders of magnitude larger than the magnetic signal from targets and must be culled from data sets prior to interpretation. Suppression of the powerline noise by simple filtering can result in artifacts and an unacceptable reduction in resolution of ground-based and unmanned aerial vehicle magnetic surveys. Removal approaches such as those based on Biot–Savart modeling are sensitive to the estimated position of the powerline systems, in addition to their limited applicability due to the requirement of a DC source. Moreover, the powerline noise in data acquired from a moving platform is inherently nonstationary and removal techniques must be specifically developed with this in mind. We propose a model-based method that does not rely on *a priori* knowledge of the powerline system by fitting and subtracting a set of sinusoids to the data. These sinusoids are computed on small windows of data, tied together with regularization terms within the fitting process to reduce discontinuities between segments. We further incorporate powerline frequency as a nonlinear parameter, allowing for fluctuations in the fundamental frequency as loads on the power grid change. Through synthetic and field examples, we show that periodic noise can be reliably removed automatically without the need for filtering or significant alterations of the frequency content. Powerline noise is reduced by over 98% in the field example.**

***Index Terms*— Magnetic survey, powerline noise removal, signal processing.**

I. Introduction

HIGH-RESOLUTION ground and unmanned aerial vehicle (UAV)-based magnetic surveys are becoming increasingly common, as the benefits to archeological studies, environmental remediation, detection of unexploded ordnance (UXO), and local geologic investigation are evident. As examples, advanced UXO discrimination requires high spatial resolution data over small targets [1], [2], detailed archeological mapping benefits from rapid detailed surveys [3], and even a relatively simple search for abandoned well heads comprises a search for isolated targets over potentially large areas [4]. Advances in fluxgate and other magnetometry have resulted in practical systems comprising an array of sensors with high sample rates (see [4]–[8]); 100 Hz or more is easily achievable. This allows for detailed mapping applications acquired at high velocities in towed or UAV-mounted sensor configurations.

Low-bandwidth systems, i.e., with sample rates below 100 Hz, are insensitive to noise from powerlines. The powerline noise occurs at frequencies of 50 or 60 Hz (and harmonics thereof) which is either out-of-band for the magnetic sensor or the noise is removed by analog anti-aliasing filters before sampling. However, the increase in sample rates to above 100 Hz has a consequence of sampling noise from local power grids. The powerline contamination can be severe even in rural environments, with amplitudes of thousands of nanotesla (nT). With many surveys containing signals of interest less than 10 nT, the need to reliably remove the powerline noise is clear.

Frequency filtering is an obvious choice in powerline noise removal; however, with high acquisition speeds filtering can result in unacceptable reduction in resolution. Consider an acquisition speed of 20 km/h; the apparent wavelength of a 50 Hz signal is 11 cm. With sample rates exceeding 200 Hz, low-pass filtering of powerline noise can result in a factor of 10 reduction in possible spatial resolution, which can be exacerbated by the rolloff properties of the designed filter. Additionally, filtering may produce unwanted Gibbs phenomena from sharp changes in signal amplitude, especially if a notch filter is employed. In either case, frequency filtering can unacceptably alter desired anomalies in a wide spatial range.

Model-based removal of powerline noise from magnetic data offers an alternative approach which does not suffer from the limitations of frequency filtering. Previous approaches, for example [9], fit DC powerline magnetic-field effects through a Biot–Savart approach. However, full solutions of the fields generated by the powerline itself are strongly sensitive to the *a priori* placement of the powerlines themselves, and current methods are not generalized to time-varying fields.

Modeling and subtraction of 50-/60-Hz powerline noise has been successfully applied to seismic and other geophysical data as in, e.g., [10]–[14]. Periodic powerline noise is parameterized as a sum of sinusoids and cast as an inverse problem. The resultant fits are subtracted from the data, leaving the surrounding frequency content intact. This has the benefit of removal of the powerline noise while minimally affecting the signals of interest. Such methods of model-based removal

Manuscript received June 12, 2020; revised September 21, 2020; accepted October 5, 2020. Date of publication October 30, 2020; date of current version July 22, 2021. This work was supported by the Innovation Fund Denmark through the MapField and rOpen projects. *(Corresponding author: M. Andy Kass.)*

M. Andy Kass, Anders Vest Christiansen, and Esben Auken are with the Hydrogeophysics Group, Aarhus University, 8000 Aarhus, Denmark (e-mail: andy.kass@geo.au.dk).

Jakob Juul Larsen is with the Department of Engineering, Aarhus University, 8200 Aarhus, Denmark.

Digital Object Identifier 10.1109/TGRS.2020.3029658

are not sensitive to the position of the powerline; indeed no *a priori* knowledge of the power grid system is required.

We extend these methods to magnetic data acquired from a moving platform and specifically address the nonstationarity of powerline noise inherent in long data sets extending over many seconds or minutes. Direct estimation of the constituent parameters is done entirely in the time domain, avoiding Fourier operations. As a consequence, the method is insensitive to uneven sample rates, data dropouts (within reason), and time-varying powerline signal parameters. The proposed method is applicable to any periodic noise, or indeed generalized to any noise that can be represented parametrically, for example, variable electric motor noise from UAV platforms.

Multiple formulations of increasing complexity are presented based on a single philosophical approach to handle increasingly difficult scenarios, e.g., a varying fundamental frequency. We compare and contrast each method and discuss the applicability of each and present synthetic and field examples as demonstrations.

II. Theory

We cast the task of fitting powerline noise as an inverse problem. In the following, we describe both linear and nonlinear approaches utilizing windows and all-at-once (AAO) methods to account for increasingly complicated powerline signals.

Data are assumed to be acquired from a moving platform, and a single data set consists of multiple linear or sublinear segments (lines) covering an area of interest. These lines can be treated as independent time series, containing any component of the magnetic field or gradient.

A. Linear Windowed Approach

The windowed approach breaks each line (time series) of data into short segments, for example 1 s, where the fundamental frequency, phase, and amplitude of the powerline signal is assumed constant. Within each window, a set of sinusoids is fit to the data, resulting in an estimate of amplitude and phase for the fundamental frequency, f_p, and each subsequent harmonic of interest. In the following, we use the standard rewriting $a\cos(2\pi f t + \theta) = A\cos(2\pi f t) + B\sin(2\pi f t)$ with $a = (A^2 + B^2)^{1/2}$ and $\tan\theta = -B/A$, where a is amplitude, θ phase, and t time, to remove the nonlinear dependence on phase. The powerline contribution, d_{pl}, is here presented as two sinusoids, one for the fundamental 50-Hz signal and one for the first harmonic at 100 Hz (as our specific instrument samples up to 230 Hz), however, the approach is general for an arbitrary number of harmonically related sinusoidal components, $i_{\max}$

$$\mathbf{d}_{\mathrm{pl}} = \sum_{i=1}^{i_{\max}} A_i \cos\left(2i\pi f_p \mathbf{t}\right) + B_i \sin\left(2i\pi f_p \mathbf{t}\right). \quad (1)$$

Let $\mathbf{d}$ represent a time-series data vector, for example, total field or some other magnetic or gradient component. The observed data vector can be represented as the sum of its constituent noise components as

$$\mathbf{d} = \mathbf{d}_{\mathrm{signal}} + \mathbf{d}_{\mathrm{pl}} + \varepsilon \quad (2)$$

where $\mathbf{d}_{\mathrm{signal}}$ represents the magnetic signal of interest, and ε a random noise vector, assumed uncorrelated with the powerline signal.

For a fixed powerline frequency, the powerline contribution, d_{pl}, can be cast as a linear system with unknown parameters A_i and B_i

$$\mathbf{Gm} = \mathbf{d} \quad (3)$$

where

$$\mathbf{G} = \begin{bmatrix} \cos\left(2\pi f_p t_1\right) & \sin\left(2\pi f_p t_1\right) & \cos\left(4\pi f_p t_1\right) & \sin\left(4\pi f_p t_1\right) \\ \cos\left(2\pi f_p t_2\right) & \sin\left(2\pi f_p t_2\right) & \cos\left(4\pi f_p t_2\right) & \sin\left(4\pi f_p t_2\right) \\ \vdots & \vdots & \vdots & \vdots \\ \cos\left(2\pi f_p t_k\right) & \sin\left(2\pi f_p t_k\right) & \cos\left(4\pi f_p t_k\right) & \sin\left(4\pi f_p t_k\right) \end{bmatrix}$$

$$\mathbf{m} = [A_1 \ B_1 \ A_2 \ B_2]^T$$

$$\mathbf{d} = [d_1 \ d_2 \ \ldots \ d_k]^T$$

and k the number of observed data. We note that this implicitly assumes the powerline contribution is the dominant source of 50-Hz energy in the system.

We can solve for a parameter vector $\mathbf{m}$ for each window in a least squares sense via

$$\mathbf{G}^T\mathbf{Gm} = \mathbf{G}^T\mathbf{d} \quad (4)$$

using any suitable linear solver such as the Conjugate Gradient method (see [15]). The resulting parameters are then used to create a set of predicted powerline data $\mathbf{d}_{\mathrm{pl}}$ which is subsequently subtracted from the observed signal as in (2). We use an exhaustive parameter search to identify f_p. To solve the system, we model a sweep of frequencies, usually between 49.9 and 50.1 Hz, and select the f_p resulting in the lowest data misfit [13].

The windowed approach explicitly assumes that the 50-Hz noise is stationary within each segment. In a real survey, even 1 s of data may be too long and violate this assumption. Moreover, acquiring data from a moving platform further adds a temporal component. However, reducing the window size means reducing the number of cycles available for fitting and can destabilize the procedure. We therefore use a two-step approach, whereby a longer window of 1 or 2 s is used to obtain an initial guess for a second pass with a shorter window, for example 0.1 s. The initial guess, used as a starting and/or reference model stabilizes the solution in spite of the larger condition number of the system.

Independent construction of model parameters in each window of data will often lead to discontinuities in the recovered model parameters. These can map into the denoised data as discontinuities in the first derivative, and less frequently as jumps in the data themselves. To control this effect, we turn to a regularized inverse approach.

B. All-at-Once Approach

Although the windowed approach can work well in many cases where the noise levels are low and the powerline noise changes slowly, discontinuities and large changes in signal properties can negatively affect the parameter estimates. Ideally, the recovered sinusoid amplitudes as well as the estimated frequency should be allowed to smoothly change as a function of time. Moreover, the desired signal, $\mathbf{d}_{\text{signal}}$, is not devoid of 50-Hz energy. Regularization can control and prevent the overfitting of this 50-Hz energy in the $\mathbf{d}_{\text{signal}}$ component. By solving a large system containing the entire line of data, we can introduce a smoothness term between the model parameters. In the linear inverse case (i.e., f_p is not included as an unknown parameter), f_p is either fixed or assumed known as a function of time.

We continue with the philosophy of utilizing windows of data where the model parameters are assumed constant. With a window length of greater than 4 samples, the system remains overdetermined and regularization is not explicitly required, though can be applied. As the window length decreases, the conditioning of the system is worsened, and in the extreme case—as the number of samples per window decreases to less than 4—the system becomes underdetermined and regularization is required. Regularization in our context is achieved through the use of derivative terms which improve the condition number and introduce an *a priori* estimate of smoothness.

For clarity, we first construct the new system of equations based on (4) without a regularization term; we then apply a Tikhonov-based scheme [16] and present the solution. In order to construct one linear system for an entire line of data consisting of q windows, we cast (3) as a block sparse system

$$\begin{bmatrix} \mathbf{G}_1 & & & \\ & \mathbf{G}_2 & & \\ & & \ddots & \\ & & & \mathbf{G}_q \end{bmatrix} \begin{bmatrix} \mathbf{m}_1 \\ \mathbf{m}_2 \\ \vdots \\ \mathbf{m}_q \end{bmatrix} = \begin{bmatrix} \mathbf{d}_1 \\ \mathbf{d}_2 \\ \vdots \\ \mathbf{d}_q \end{bmatrix} \tag{5}$$

where each $\mathbf{G}_i$, $\mathbf{m}_i$, and $\mathbf{d}_i$ is exactly equivalent to the definition of a single window solution as described in 4. The solution of (5) is again exactly equivalent to solving (3) for each window independently for equivalent window sizes. In order to leverage smoothness, we introduce Tikhonov regularization.

The solution of (4) is equivalent to minimizing a single-term objective function given by

$$\phi_d = \|\mathbf{W}_d(\mathbf{G}\mathbf{m} - \mathbf{d}_{\text{obs}})\|_2^2 \tag{6}$$

where $\mathbf{W}_d$ represents a data weighting matrix containing the reciprocals of the estimated data standard deviations along the diagonal. We seek to add a second term containing a squared model norm such that the objective function, Φ, becomes

$$\Phi = \phi_d + \beta\phi_m \tag{7}$$

where β is a yet-unknown tradeoff parameter and ϕ_m contains any *a priori* information about the model such as smoothness or a reference model. In the simplest case, ϕ_m is given by

$$\phi_m = \|\mathbf{m}\|_2^2 \tag{8}$$

favoring solutions with the smallest recovered model parameters. We can generalize (8) to include a reference model and any model weighting we wish, such as minimizing the first derivative, through incorporation of a reference model and model weighting matrix (Appendix A)

$$\phi_m = \|\mathbf{W}_m(\mathbf{m} - \mathbf{m}_{\text{ref}})\|_2^2. \tag{9}$$

It is in this weighting matrix, $\mathbf{W}_m$, that we incorporate smoothness terms, while $\mathbf{m}_{\text{ref}}$ constitutes the reference model, either implicitly zero or containing the recovered parameters from the solution using larger window sizes.

After construction of the model weighting matrix, the linear system to be solved in (4) becomes

$$\begin{aligned}\left(\mathbf{G}^T\mathbf{W}_d^T\mathbf{W}_d\mathbf{G} + \beta\mathbf{W}_m^T\mathbf{W}_m\right)\mathbf{m} \\ = \mathbf{G}^T\mathbf{W}_d^T\mathbf{W}_d\mathbf{d}_{\text{obs}} + \beta\mathbf{W}_m^T\mathbf{W}_\mathbf{m}\mathbf{m}_{\text{ref}}\end{aligned} \tag{10}$$

which can similarly be solved with any appropriate sparse linear solver [15], [17].

C. Inclusion of the Fundamental Frequency as an Unknown Parameter

We may include the fundamental frequency f_p as an unknown parameter at the expense of making the system nonlinear. Despite this complication, the nonlinear solution can reduce the computational load significantly as the frequency parameter need not be exhaustively searched. Experiments show that four to six linearized solutions replace a parameter sweep requiring potentially many linear solutions. More significantly, the estimates of the fundamental frequency are improved.

We again formulate the solution with Tikhonov regularization, adding in frequency as a free parameter. The system can be solved with any nonlinear method; we present a Gauss–Newton method here [15].

The formulation is similar to (10), but is instead iteratively solved for a model update, $\delta\mathbf{m}$, with linearized steps. Each iteration solves the linear equation

$$\begin{aligned}&\left(\mathbf{J}^T\mathbf{W}_d^T\mathbf{W}_d\mathbf{J} + \beta\mathbf{W}_m^T\mathbf{W}_m\right)\delta\mathbf{m} \\ &= \mathbf{J}^T\mathbf{W}_d^T\mathbf{W}_d\left(\mathbf{d}_{\text{obs}} - F\left[\mathbf{m}^{(n)}\right]\right) \\ &\quad - \beta\mathbf{W}_m^T\mathbf{W}_m\left(\mathbf{m}^{(n)} - \mathbf{m}_{\text{ref}}\right)\end{aligned} \tag{11}$$

with

$$\mathbf{m}^{(n+1)} = \mathbf{m}^{(n)} + \delta\mathbf{m} \tag{12}$$

where $\mathbf{J}$ is a Jacobian matrix explicitly defined in Appendix B, $F[\cdot]$ is the forward model operator which maps an element from the model space to the data space, given by (3), and $\mathbf{m}^{(n)}$ is the recovered model at the nth iteration (see [18]).

D. Selection of Tradeoff Parameter

Inclusion of model weighting in an overdetermined system results in challenges in selection of tradeoff parameter, β. In an overdetermined case, the optimal value of β is zero; the addition of regularization necessarily will increase the data misfit value, ϕ_d. Selection criteria such as the L-curve [19] or generalized cross validation (see [16]) will drive the recovered β to zero, while discrepancy principle approaches based on ϕ_d (see [17]) are invalid as the "optimum" misfit is undefined. Since the definition of smoothness in model parameters between windows is somewhat arbitrary, so will be the choice of β. We suggest choosing a β such that the frequency spectrum is maximally flat in the range of 50 Hz and harmonics after subtraction of the computed powerline model. This prevents overfitting of the 50-Hz signal present in magnetic anomalies.

III. Examples

A. Synthetic Example

We simulated a set of synthetic total-field data comprising the signals from 11 dipoles of varying depths and magnetizations, selected to represent signals as varied as small, near-surface ferrous targets (as shallow as 0.5 m) to deeper geologic sources (at 500-m depth). In magnetic data, the depth of the source behaves as a low-pass filter, thus the deeper sources result in broader or longer-wavelength anomalies. The data simulate one acquisition line sampled at 225 Hz with a 5-m/s driving speed for 100 s, or 500 m, with a powerline positioned at 300 m perpendicular to driving direction whose signal decays as distance-squared. The fundamental frequency smoothly changes with time following a sinusoidal drift pattern: $f_p = 50 + 0.01 \sin(2\pi/100t)$. For visual clarity, additional noise (e.g., Gaussian) is not shown in this particular simulation, but does not materially affect the final result. We included the first harmonic at 1% of the fundamental amplitude to match empirical observations. In these simulations, we used a window length of 100 ms.

Fig. 1 shows the results from the four methods as described. In general, the windowed approaches have superior removal of powerline signal in between the anomalies (i.e., in windows containing only a sinusoidal signal), while the AAO methods affect the anomalies of interest less. Depending on the target anomaly amplitude, the error introduced through the use of this method is acceptable—predominantly under 1 nT. Larger misfits occur directly over magnetic targets; this is due to overfitting of the 50 Hz signal inherently present in broadband magnetic anomalies. In general, the powerline contribution is reduced to between 0.5% and 2% of its former amplitude.

As the exact noise contribution is known in the synthetic case, we compute the energy of the real and predicted powerline signal before and after processing. The energy, E, of a signal $f(t)$ over an interval $[t_1, t_2]$ is given by

$$E = \int_{t_1}^{t_2} |f(t)|^2 \, dt. \tag{13}$$

The difference of the energy loss between the true and predicted powerline signal divided by the energy of the true signal yields an estimate of recovery error, which vary between 0.007% and 0.069% depending on the method.

There exists an ambiguity between frequency and phase in the recovered solutions. This is exacerbated when the powerline frequency is estimated first and not allowed to vary within the inverse solution. The effect can be seen in Fig. 1(a), for example, where large discontinuities are required in the phase to fit the data given a fixed f_p.

TABLE I

Field Example Inversion Parameters for Linear (L) and Nonlinear (NL) Windowed and AAO Solutions. See Appendix A for a Full Description of the Alpha Parameters

	Window [mS]	β	α_c	α_f	α_{dc}	α_{df}
L Windowed	250	0	NA	NA	NA	NA
L AAO	250	1e-6	0.01	NA	1	NA
NL Windowed	250	90	0.001	5	NA	NA
NL AAO	100	90	1e-4	5	1e-4	1e-6

B. Field Example

We present a field example from an archeological site near Ørregård, Denmark. The field site contains a high-tension powerline crossing subperpendicularly to the acquisition lines which induced at maximum an approximate 1000-nT signal into the data, compared to a much smaller 10–50-nT signal from the archeological remains.

Data were acquired with the tMag system (https://hgg.au.dk/instruments/tmag/) utilizing vector magnetic sensors in a gradient configuration towed 10 m behind an all-terrain vehicle (ATV). The array consists of eight vertical magnetic gradiometers, each utilizing two sets of three-component fluxgate sensors, separated horizontally by 50 cm broadside to the driving direction and 1 m vertically. Positioning is achieved through two roving differential GPS units mounted on the frame and one base station GPS near the survey area. Acceleration and attitude information is recorded with an inertial measurement unit also mounted on the frame. Data were sampled at 225 Hz with a nominal driving speed of 18 km/h, maximum 20 km/h. Nominal line spacing was 2.25 m to ensure full coverage on the field, though significant variation exists due to driving conditions. All data components were acquired; we show the total field data as an example.

The survey was conducted as an archeological investigation of an iron-age settlement. Fortunately, the primary area of interest was south of the most significant powerline interference; however, the large amplitudes of the signal interfered with the bias corrections so harmonic removal was nonetheless necessary. We note that the 50-Hz signal is present throughout the geographical area of the survey.

The raw data first had relevant gain corrections applied. Then each of the harmonic removal methods was applied according to the parameters listed in Table I. Results for a single sensor along a single line are shown in Fig. 2, with detailed windows shown in 3. For map plotting (Fig. 4), data were subsequently processed with a windowed (30 m) bias calculation and gridded with an inverse-distance weighting algorithm at a 0.1 m cell size.

Each of the described methods adequately removes the 50-Hz noise from the data; over 98% of the powerline amplitude is removed. Because the total signal varies smoothly, there is little difference between the recovered solutions; in fact it is difficult to choose a 'best' method based solely on line results.

It is illustrative to compare the recovered models between the linear and nonlinear solutions. In the linear case [Fig. 2(a) and (b)], f_p is fixed, yet it and phase are inextricably linked,

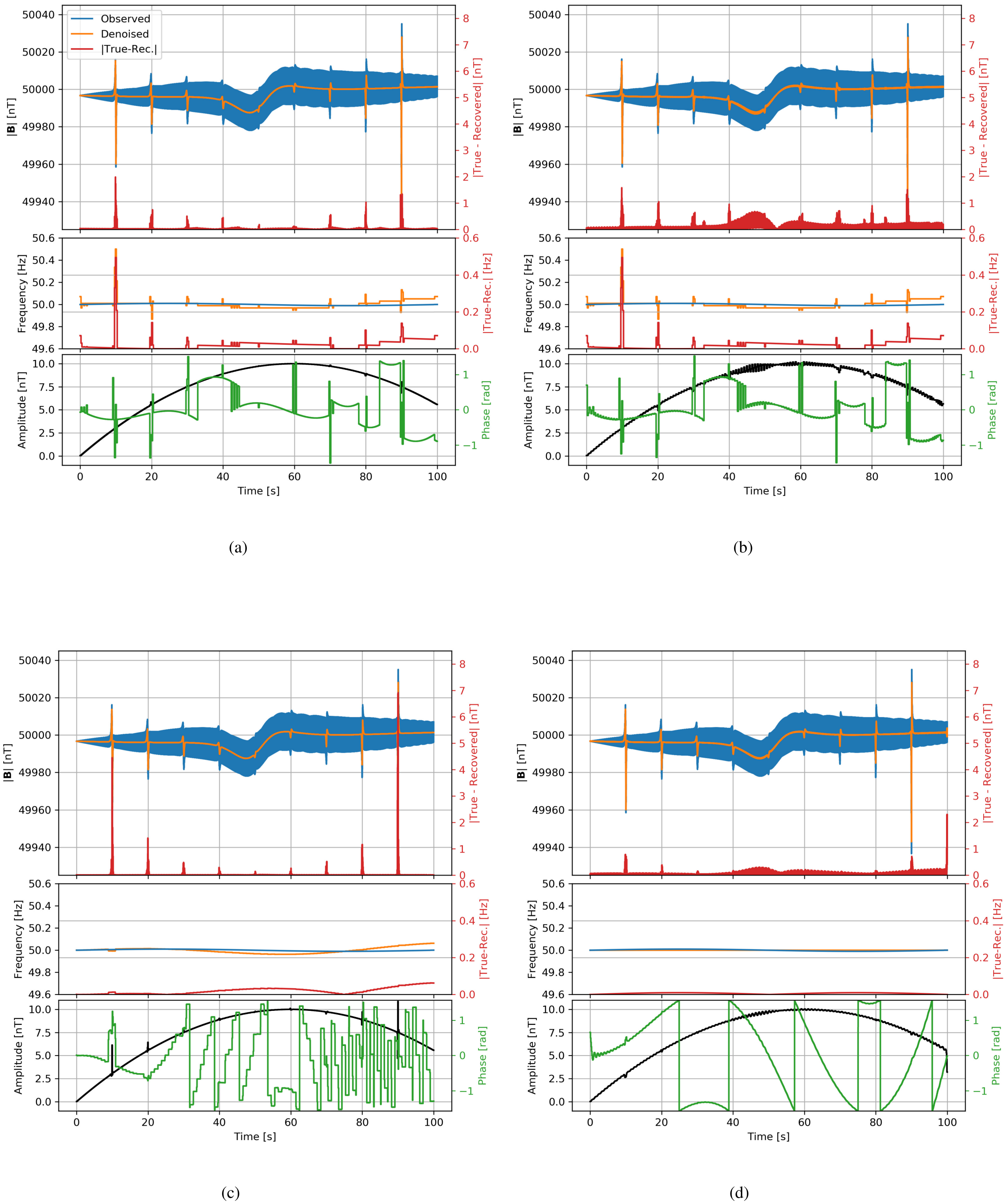

Fig. 1. Synthetic results. (Top) Simulated observed data in blue with the recovered data overlain. The absolute value of the difference between the two curves is shown in red corresponding to the axis on the right. (Middle) True and recovered fundamental frequency with the same color scheme. (Bottom) Recovered amplitude and phase for each solution method. The windowed approaches have superior removal of powerline signal between the anomalies, while the AAO approaches are more faithful to the magnetic signature of the modeled dipoles. (a) Linear windowed. (b) Linear AAO. (c) Nonlinear windowed. (d) Nonlinear AAO.

so variability in f_p will necessitate corresponding changes in phase. This severely restricts the amount of smoothing possible. In contrast, the phase shows fewer discontinuities across the line in the nonlinear solutions [Fig. 2(c) and (d)]. For the same reasons, the linear windowed and AAO solutions are similar, as the algorithm has a limited ability to adjust

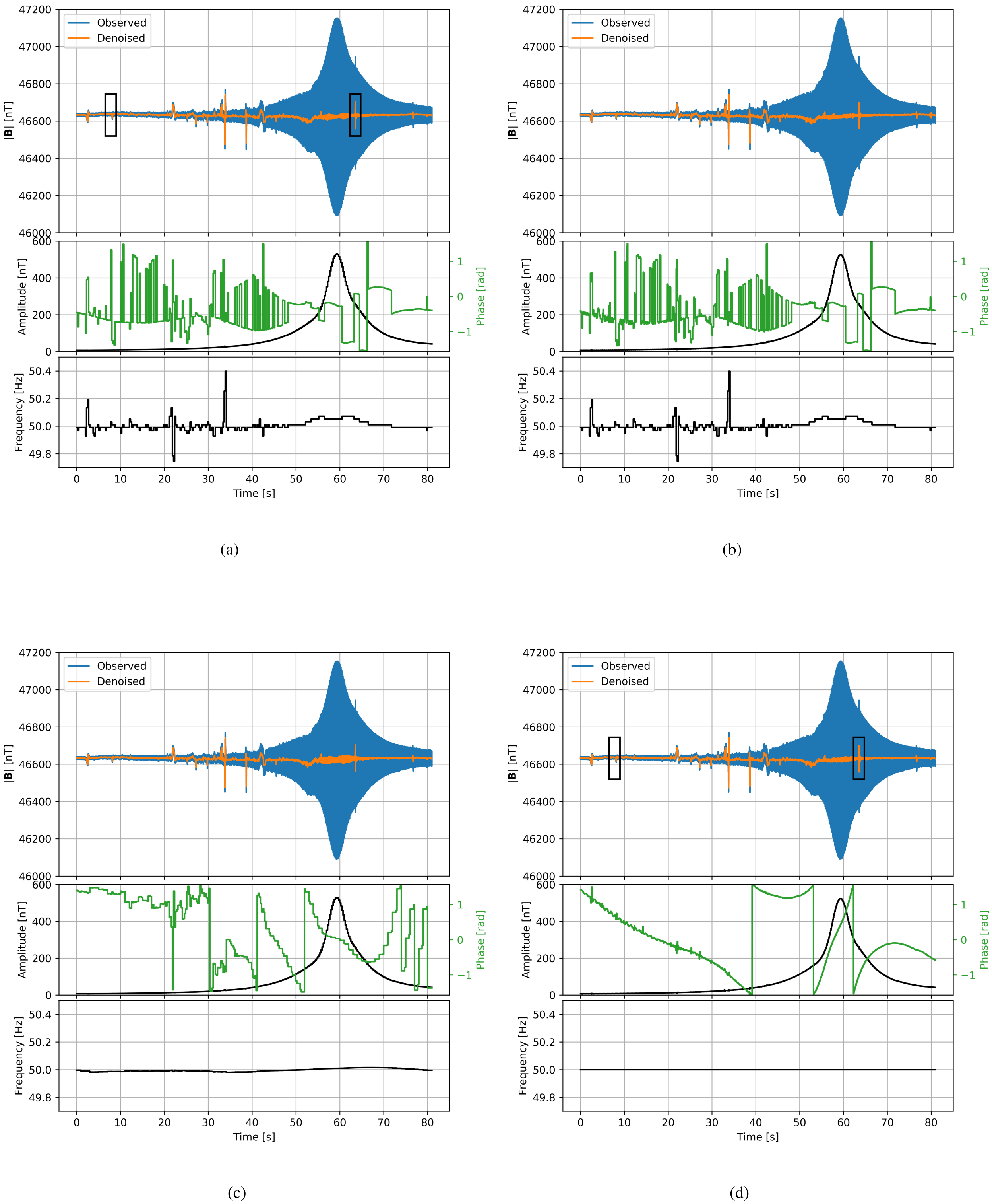

Fig. 2. Ørregård field example results. (a) Linear, windowed solution. (b) Linear AAO solution, using the same frequencies as (a). Differences between the two linear solutions are within ±2 nT. (c) Nonlinear, windowed solution with frequency as a free parameter. (d) Nonlinear, AAO solution. Black boxes in (a) and (d) correspond to the zoomed data plots shown in in Fig. 3

phase. However, the linear AAO solution has slightly better noise characteristics relative to the windowed case.

The frequency spectra comparison before and after processing demonstrates the usefulness of the technique. Care must

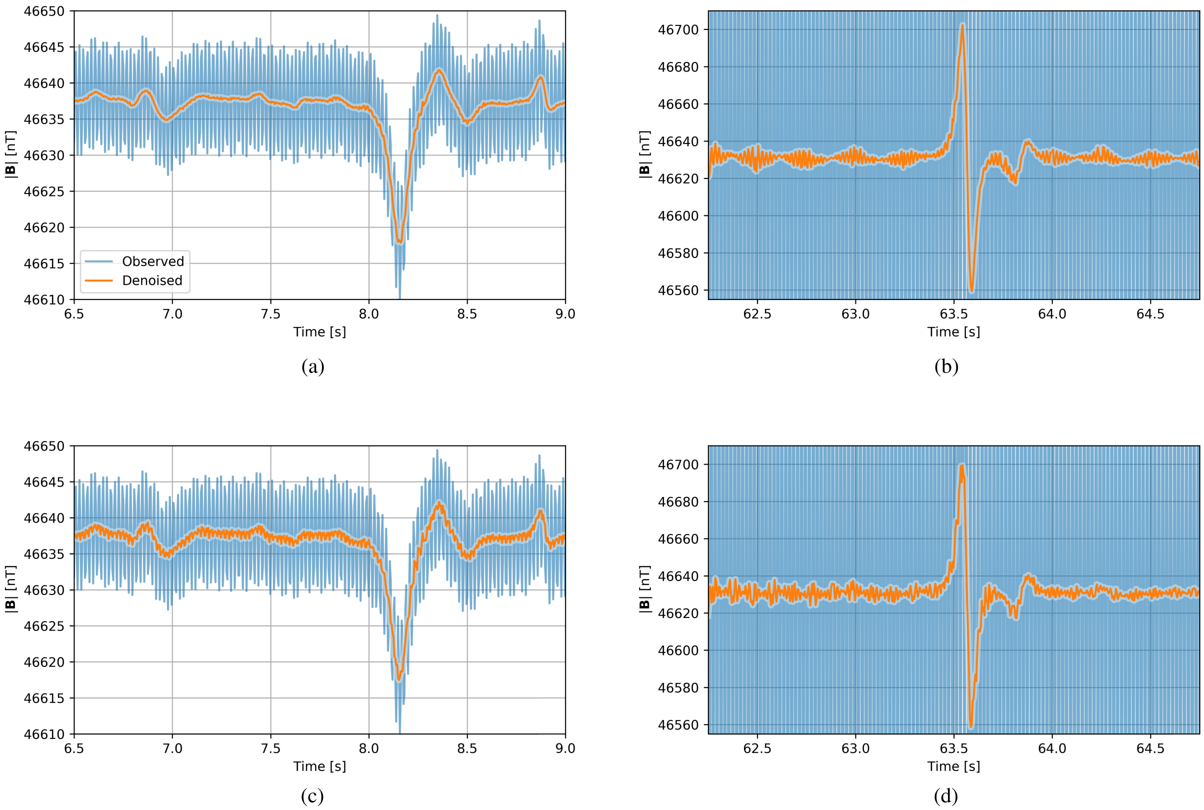

Fig. 3. Inset data from Fig. 2. The powerline contribution has been reduced over 98%, though some beating still remains due to a slight offset in modeled frequency. (a) Inset 1 from Fig. 2(a). (b) Inset 2 from Fig. 2(a). (c) Inset 1 from Fig. 2(d). (d) Inset 2 from Fig. 2(d).

be taken, however, as the Fourier transform of an entire line of data violates required assumptions about stationarity. We therefore show the transforms (amplitude spectra) of a single window of data, where we previously have assumed stationarity within that timescale. Fig. 5 shows the results of such a window in the region of the strongest powerline signal before and after processing. The observed data are dominated by the 50-Hz signal, while the post processed data are consistent with an amplitude spectrum expected of magnetic gradient data of this type. We note that we have overfit the 50-Hz signal slightly, showing the usefulness of examining the spectra in selecting an optimal tradeoff.

Fig. 4 shows gridded data before and after processing with the nonlinear AAO technique. Note the large signal contamination from the powerline, extending from southeast to northwest, in Fig. 4(a). This signal is eliminated in Fig. 4(b). Not only does this ease visual interpretation in the areas adjacent to the powerline, but also eliminates much of the artifacts from the subsequent bias-correction processing step caused by the large noise amplitude [striping seen parallel to the long axis of the survey in Fig. 4(a)].

IV. Discussion

Each of the four methods described here has advantages and disadvantages. Although the windowed approaches generally have a lower remaining 50-Hz content in between target anomalies, they underperform at the anomalies themselves. The opposite is true for the AAO solutions. The anomalies from magnetic targets have a broadband signal in the Fourier domain, including a 50-Hz component. Regularization in the AAO methods helps to avoid overfitting the 50-Hz component in these areas. In deference to the need for a minimum of distortion in these targets, we prefer the nonlinear AAO approach, especially if one plans to do further detailed processing such as parametric inversion (see [20]).

Both the windowed and AAO approaches have similar performance in terms of speed; however the AAO is generally slightly faster as there is less overhead in memory management. Comparison between the linear and nonlinear solutions depends on how exhaustively the fundamental frequency is searched at the beginning of the linear solution; if f_p is coarsely estimated, the linear solution can be four or five times faster than the nonlinear approach. A 100-s line of data takes approximately 4–6 s to process for nonlinear AAO solutions on an i7 processor (the algorithms are written in Python 3.6), whereas the linear cases take roughly double the time including the frequency search of 100 frequencies. The entire field survey shown here ran in approximately six minutes. We note that we use sparse matrix operations to conserve memory, which can have an impact on efficiency.

In the examples shown here, we processed each of the eight gradiometer packages independently. While the timing is accurately controlled, each sensor package is on an independent

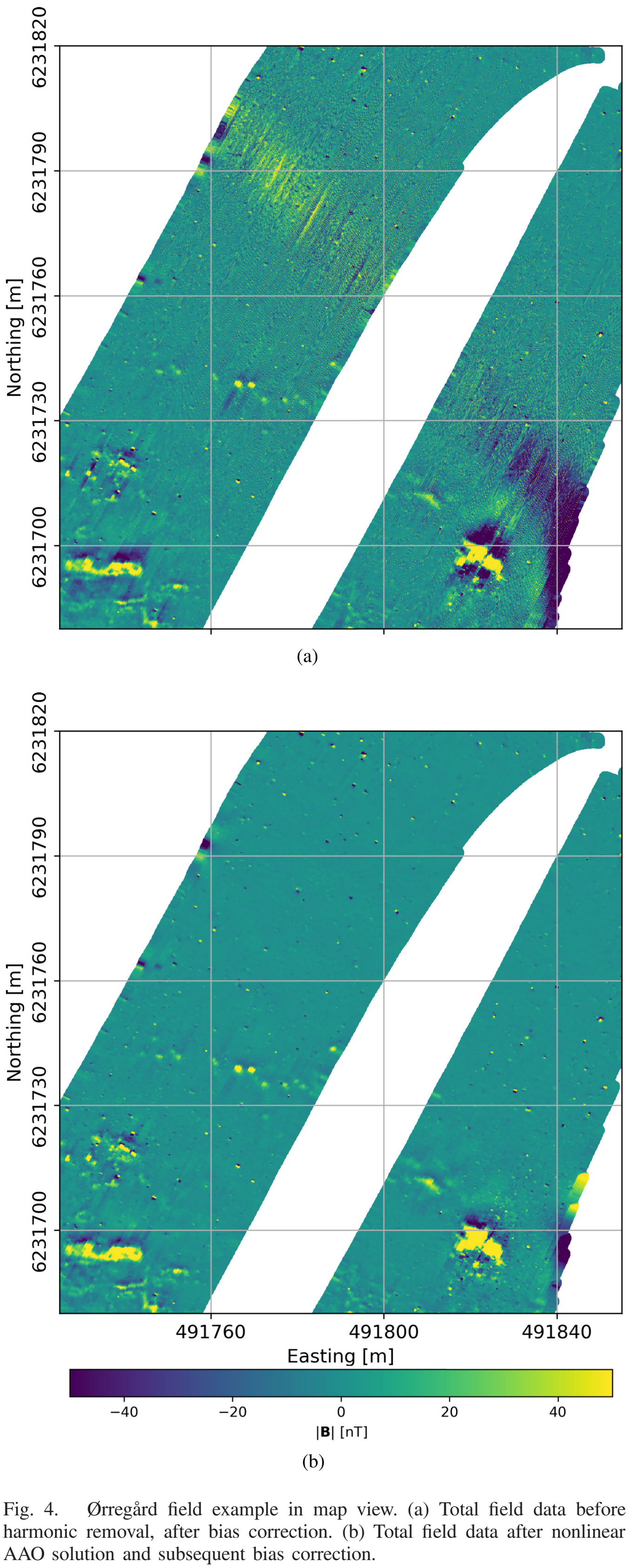

Fig. 4. Ørregård field example in map view. (a) Total field data before harmonic removal, after bias correction. (b) Total field data after nonlinear AAO solution and subsequent bias correction.

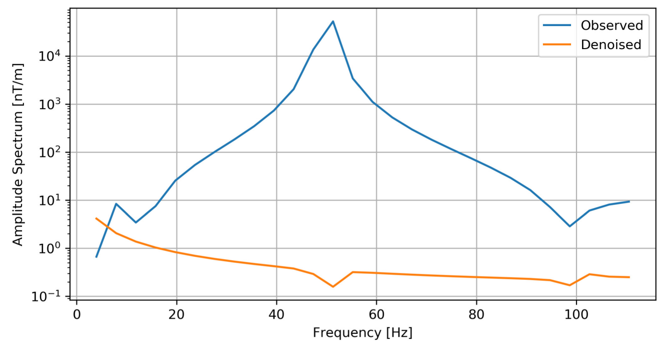

Fig. 5. Amplitude spectra of a single window of data near the powerline source before and after processing.

hardware clock; for systems built around a master clock, the performance can be further improved by processing the entire array at once.

In most magnetic surveys, a base station is deployed to measure background diurnal changes in the magnetic field to be subtracted during data processing. Although the base station would ideally be placed in a noise-free area, the practical limits of many surveys preclude this. If the base station has a similar sample rate to the survey instrument, the recorded data can be used to further constrain the estimates of f_p and improve performance. Careful inspection of the remaining signal in the field data set shows beating in the regions with the strongest powerline contribution; this is due to a slight offset in the estimated f_p from the true frequency. The use of a base station may be an effective way to control this effect.

One possible alternative to solving an AAO solution is to use overlapping windows and solve each independently. The recovered parameters are then interpolated between the windows and the subsequent signal subtracted. This does not, however, adequately address the issue of overfitting 50-Hz signal in the target anomalies in general. We submit that the AAO methodology presented here is a more direct means of controlling this overfitting.

In future instrumentation with even higher sample rates, the methodology here can be trivially extended to an arbitrary number of harmonics, at the cost of processing time. For comparison, it is common in direct current/induced polarization and surface nuclear magnetic resonance processing to model several tens of harmonics.

We note that while vibrational noise is almost always below 50 Hz, translation and rotation of the sensors (if using gradient or vector data) will result in further nonstationary characteristics of the signal. The coupling of the powerline into the sensor will change over timescales less than practical window lengths. We control the effect through correction with an inertial measurement system; however application of the methods described here on instruments without this capability will benefit from further study.

The examples shown in this article focus on powerline signals, but indeed the methods presented are equally applicable to any periodic signal. In fact, so long as the signal to be removed is capable of being represented parametrically, the method holds. We foresee strong applications in the emerging field of drone magnetometry, where variable noise from the electric motors on UAVs can be removed using this method.

V. Conclusion

We have developed a methodology for rapid attenuation of powerline influences in magnetic data through a model-based approach. By fitting and removing windowed sinusoidal signals from the data, we can reduce the powerline contribution by over 98%, as seen in the synthetic and field examples. This method does not require any *a priori* knowledge of the powerline parameters, including spatial location. In addition, the method does not rely on frequency filtering, meaning no Fourier-introduced aberrations are present. We propose that the nonlinear AAO method presented here is in general the best technique for powerline removal when considering the tradeoff between minimizing distortion of target anomalies versus maximum signal removal in anomaly-free regions.

Appendix A
Explicit Formulation of the Model Weighting Matrices

The model weighting matrix used in both the linear and nonlinear solutions is an aggregate matrix formed by the sum of its constituents

$$\mathbf{W}_m = \sum \alpha_i \mathbf{W}_i \tag{14}$$

where α_i is a scalar weighting term.

The matrices corresponding to the reference model are diagonal with ones on the elements corresponding to the relevant parameters. In this application, we usually weight the cosine terms (α_c) equally, and the frequency term (α_f) a few orders of magnitude higher. For the case with five parameters given as

$$\mathbf{m} = [A_1 \;\; B_1 \;\; A_2 \;\; B_2 \;\; f]^T \tag{15}$$

the aggregate matrix is constructed as

$$\mathbf{W}_p = \mathrm{diag}\big(\alpha_c \;\; \alpha_c \;\; \alpha_c \;\; \alpha_c \;\; \alpha_f\big). \tag{16}$$

For the AAO approach, the diagonal would be repeated for as many windows as are present.

The AAO approach can also include derivative terms in a finite-difference or finite-element sense, $\mathbf{W}_{\mathrm{dc}}$ and $\mathbf{W}_{\mathrm{df}}$. Using (15)

$$\mathbf{W}_{\mathrm{dc}} = \begin{bmatrix} 1 & 0 & 0 & 0 & 0 & -1 & \\ & 1 & 0 & 0 & 0 & 0 & -1 \\ & & & & & & \ddots \end{bmatrix} \tag{17}$$

with every fifth row equaling zero, corresponding to the frequency terms. $\mathbf{W}_{\mathrm{df}}$ has an equivalent structure, however, with every fifth row comprising the only nonzero elements. The aggregate model weighting matrix from (16) and (17) is therefore

$$\mathbf{W}_m = \mathbf{W}_p + \alpha_{\mathrm{dc}}\mathbf{W}_{\mathrm{dc}} + \alpha_{\mathrm{df}}\mathbf{W}_{\mathrm{df}}. \tag{18}$$

Appendix B
Explicit Jacobian Formulation

The nth column of the Jacobian $\mathbf{J}_n$ can be analytically formulated as follows:

$$\mathbf{J}_0 = \cos(2\pi f \mathbf{t}) \tag{19}$$
$$\mathbf{J}_1 = \sin(2\pi f \mathbf{t}) \tag{20}$$
$$\mathbf{J}_2 = \cos(4\pi f \mathbf{t}) \tag{21}$$
$$\mathbf{J}_3 = \sin(4\pi f \mathbf{t}) \tag{22}$$
$$\begin{aligned}\mathbf{J}_4 = & -2\pi A_1 \mathbf{t} \sin(2\pi f \mathbf{t}) \\ & + 2\pi B_1 \mathbf{t} \cos(2\pi f \mathbf{t}) \\ & - 4\pi A_2 \mathbf{t} \sin(4\pi f \mathbf{t}) \\ & + 4\pi B_2 \mathbf{t} \cos(4\pi f \mathbf{t})\end{aligned} \tag{23}$$

where $\mathbf{t}$ is a vector of times corresponding to the data vector $\mathbf{d}$ such that

$$\mathbf{d} = F[\mathbf{m}(\mathbf{t})]. \tag{24}$$

Acknowledgment

The authors would like to thank Museum Midtjylland, especially Mikkel Fugelsang and Line Jørgensen for site access, field help, data comparison, and background information. They also thank the anonymous reviewers whose suggestions improved this article.

References

[1] S. D. Billings, "Discrimination and classification of buried unexploded ordnance using magnetometry," *IEEE Trans. Geosci. Remote Sens.*, vol. 42, no. 6, pp. 1241–1251, Jun. 2004.

[2] B. Barrow and H. Nelson, "Collection and analysis of multi-sensor ordnance signatures with MTADS," *J. Environ. Eng. Geophys.*, vol. 3, no. 2, pp. 49–100, 1998.

[3] N. Linford, P. Linford, and A. Payne, "Advanced magnetic prospecting for archaeology with a vehicle-towed array of cesium magnetometers," in *Innovation in Near-Surface Geophysics: Instrumentation, Application, and Data Processing Methods*, R. Persico, S. Piro, and N. Linford, Eds. Amsterdam, The Netherlands: Elsevier, 2019, ch. 5, pp. 121–149.

[4] G. Veloski, R. Hammack, J. Sams, III, L. Wylie, and K. Heirendt, "Evaluation of the micro-fabricated atomic magnetometer deployed from a small autonomous rotorcraft for locating legacy oil and gas wells," in *Proc. SAGEEP*. Nashville, TN, USA: Environmental Engineering Geophysical Society, Mar. 2018, p. 8.

[5] B. Gavazzi, P. Le Maire, M. Munschy, and A. Dechamp, "Fluxgate vector magnetometers: A multisensor device for ground, UAV, and airborne magnetic surveys," *Lead. Edge*, vol. 35, no. 9, pp. 795–797, Sep. 2016.

[6] P. Ripka and P. Kaspar, "Portable fluxgate magnetometer," *Sens. Actuators A, Phys.*, vol. 68, nos. 1–3, pp. 286–289, Jun. 1998.

[7] H. H. Nelson and J. R. McDonald, "Multisensor towed array detection system for UXO detection," *IEEE Trans. Geosci. Remote Sens.*, vol. 39, no. 6, pp. 1139–1145, Jun. 2001.

[8] M. Munschy, D. Boulanger, P. Ulrich, and M. Bouiflane, "Magnetic mapping for the detection and characterization of UXO: Use of multi-sensor fluxgate 3-axis magnetometers and methods of interpretation," *J. Appl. Geophys.*, vol. 61, nos. 3–4, pp. 168–183, Mar. 2007.

[9] M. Gharibi and L. B. Pedersen, "Removal of DC power-line magnetic-field effects from airborne total magnetic-field measurements," *Geophys. Prospecting*, vol. 48, no. 3, pp. 617–627, May 2000.

[10] K. E. Butler and R. D. Russell, "Subtraction of powerline harmonics from geophysical records," *Geophysics*, vol. 58, no. 6, pp. 898–903, Jun. 1993.

[11] J. Xia and R. D. Miller, "Design of a hum filter for suppressing power-line noise in seismic data," *J. Environ. Eng. Geophys.*, vol. 5, no. 2, pp. 31–38, Jun. 2000.

[12] K. E. Butler and R. D. Russell, "Cancellation of multiple harmonic noise series in geophysical records," *Geophysics*, vol. 68, no. 3, pp. 1083–1090, May 2003.

[13] J. J. Larsen, E. Dalgaard, and E. Auken, "Noise cancelling of MRS signals combining model-based removal of powerline harmonics and multichannel Wiener filtering," *Geophys. J. Int.*, vol. 196, no. 2, pp. 828–836, Feb. 2014.

[14] P.-I. Olsson, G. Fiandaca, J. J. Larsen, T. Dahlin, and E. Auken, "Doubling the spectrum of time-domain induced polarization by harmonic de-noising, drift correction, spike removal, tapered gating and data uncertainty estimation," *Geophys. J. Int.*, vol. 207, no. 2, pp. 774–784, Nov. 2016.

[15] J. Nocedal and S. Wright, *Numerical Optimization*. New York, NY, USA: Springer, 1999.

[16] R. Aster, B. Borchers, and C. Thurber, *Parameter Estimation and Inverse Problems*. Oxford, U.K.: Elsevier, 2005.

[17] D. Oldenburg and Y. Li, *Inversion for Applied Geophysics: A Tutorial*. Tulsa, OK, USA: Society Exploration Geophysicists, 2005, ch. 5, pp. 89–150.

[18] R. Parker, *Geophysical Inverse Theory*. Princeton, NJ, USA: Princeton Univ. Press, 1994.

[19] P. C. Hansen and D. P. O'Leary, "The use of the L-curve in the regularization of discrete ill-posed problems," *SIAM J. Sci. Comput.*, vol. 14, no. 6, pp. 1487–1503, Nov. 1993.

[20] S. D. Billings *et al.*, "Unexploded ordnance discrimination using magnetic and electromagnetic sensors: Case study from a former military site," *Geophysics*, vol. 75, no. 3, pp. B103–B114, May 2010.

M. Andy Kass received the B.Sc. and the Ph.D. degrees in geophysical engineering and geophysics from the Colorado School of Mines, Golden, CO, USA, in 2005 and 2012, respectively.

Following his dissertation work, he joined the Crustal Geophysics and Geochemistry Science Center, U.S. Geological Survey, Reston, VA, USA, as a Research Geophysicist, with a focus on permafrost and minerals resources. In 2017, he moved to Aarhus University, Aarhus, Denmark, to work on the development of instrumentation and interpretation methodologies, specifically focusing on magnetics, electromagnetics, and surface nuclear magnetic resonance. His research focused on the processing and inversion of multichannel electromagnetic data.

Anders Vest Christiansen received the Ph.D. degree in 2003 with a focus on airborne TEM methods and inversion methodologies.

He is an Associate Professor with the Hydrogeophysics Group, Aarhus University, Aarhus, Denmark. Overall, his research focus still remains within these subjects, in the later years with an increased focus on the integration of various data types (e.g., geophysics with borehole information and hydrological observations) with the purpose of making objective and transparent processes that generate maps and other outputs that are in better agreement with the actual needs of the end users.

Esben Auken received the M.Sc. and Ph.D. degrees in geophysics from Aarhus University, Aarhus, Denmark, in 1991 and 1996, respectively.

He is currently a Professor of geophysics with the Department of Geoscience, Aarhus University, Aarhus, Denmark. His research group, The Hydro-Geophysics Group (HGG), is 25–30 scientists all working with electrical and electromagnetic methods for high-resolution mapping of the shallow subsurface with a focus on surface and groundwater processes. He is the Co-Founder of SkyTEM Surveys Aps, Aarhus, and Aarhus Geosoftware Aps, Aarhus, both spin-out companies from the research group. HGG does high-level research on instrumental engineering, data processing, and high-performance 1-D, 2-D, and 3-D inversion algorithms. Hydrological modeling with extensive input from areal-covering geophysical measurements is an integrated part of the research. The geophysical focus areas are surface nuclear magnetic resonance (NMR), ground-based and airborne transient electromagnetics, and surface and cross borehole direct current and induced polarization. In addition, he teaches short courses for professionals and for undergraduate and postgraduate students.

Jakob Juul Larsen (Senior Member, IEEE) was born in Denmark in 1973. He received the M.Sc. and Ph.D. degrees in experimental physics from Aarhus University, Aarhus, Denmark, in 1998 and 2000, respectively.

From 2000 to 2013, he held research and teaching positions in private and public companies. Since 2013, he has been with the Department of Engineering, Aarhus University, where he is an Associate Professor. He works with geophysical instrumentation, signal processing, and machine learning. His research interests are the domains of magnetics, transient electromagnetics, direct current induced polarization, and surface nuclear magnetic resonance.